Supplementary Data

From Cluster Halides to Catalysts: Nanostructured Molybdenum Carbides for Efficient Hydrogen Evolution Reaction

Guillaume DUBOIS[1], Sébastien MATHIVET[1], Noée DUMAIT[1], Ludivine Rault[2], Stéphane CORDIER[1*], Corinne LAGROST[1,2*], Fabien GRASSET[3,4*], Franck TESSIER[1*].

[1] Univ. Rennes, CNRS, Institut des Sciences Chimiques de Rennes – UMR 6226, F-35000 Rennes, France

[2] Univ. Rennes, CNRS, ScanMAT, UAR 2025, F-35000 Rennes, France

[3] CNRS-Saint-Gobain-NIMS, IRL 3629, Laboratory for Innovative Key Materials and Structures (LINK), National Institute for Materials Science (NIMS), Tsukuba, Ibaraki, 305-0044, Japan

[4]NIMS-CNRS-Saint-Gobain International Collaboration Center, NIMS, Tsukuba, Ibaraki 305-0047, Japan

Contents

Fig. S5. Indexed SAED patterns displaying the (100), (002), (101) and (102) reflexions for Mo_2C-AHM (a), and (-111) reflexion of MoO_2 for Mo_2C-HMC (b).

Fig. S6. XPS survey spectra for Mo_2C-TMC (a), Mo_2C-HMC (b) and Mo_2C-AHM (c)

Fig. S7. Cyclic voltammetries in a non-faradaic region of the Mo_2C-AHM (a) before and (b) after 18 -chronopotentiometry at different scan rates (10, 20, 30, 40, 50, 60, 70 and 80 mV/s) in aqueous 1 M KOH.

Fig. S8. Cyclic voltammetries in a non-faradaic region of the Mo_2C-HMC (a) before and (b) after 18h-chronopotentiometry at different scan rates (10, 20, 30, 40, 50, 60, 70 and 80 mV/s) in aqueous 1 M KOH.

Fig. S9. Cyclic voltammetries in a non-faradaic region of the Mo_2C-TMC (a) before and (b) after 18h-chronopotentiometry at different scan rates (10, 20, 30, 40, 50, 60, 70 and 80 mV/s) in aqueous 1 M KOH.

Fig. S10. iR-corrected HER polarization curves in aqueous 1 M KOH at 10 mV/s for Mo_2C-TMC (bottom), Mo_2C-HMC (middle), Mo_2C-AHM (top) before and after 18h-chronopotentiometry.

Fig. S11. iR-corrected HER polarization curves normalized by ECSA in aqueous 1 M KOH at 10 mV/s for Mo_2C-TMC, Mo_2C-HMC, Mo_2C-AHM after 18h-chronopotentiometry.

Fig. S12. iR-corrected HER polarization curves normalized by mass of the catalyst in aqueous 1 M KOH at 10 mV/s for Mo_2C-TMC, Mo_2C-HMC, Mo_2C-AHM after 18h-chronopotentiometry – Mass Activity.

Fig. S13. Comparison between the XRD patterns of the AHM precursor (in blue) and that of the product (AHM + sucrose (S)) after treatment at 100°C (in orange).

Fig. S14. SEM of the precursors (AHM, TMC and HMC) before (first line) and after (second line) sucrose addition.

Fig. S15. Comparison between the XRD patterns of the TMC precursor (in blue) and that of the product (TMC + sucrose (S)) after treatment at 100°C (in orange).

Fig. S16. Comparison between the XRD patterns of the HMC precursor (in blue) and that of the product (HMC + sucrose (S)) after treatment at 100°C (in orange).

Table S1. Details of the Rietveld refinements and crystallites size for Mo_2C-AHM, Mo_2C-HMC and Mo_2C-TMC obtained with the FullProf Suite Software.

	Mo_2C-AHM	**Mo_2C-HMC**	**Mo_2C-TMC**
Lattice			
a (Å)	4.747(1)	4.726(1)	4.741(1)
b (Å)	6.004(1)	6.015(3)	6.015(2)
c (Å)	5.196(1)	5.198(1)	5.205(1)
V (Å^3)	148.1(1)	147.8(1)	148.1(1)
Space group	*Pbcn*	*Pbcn*	*Pbcn*
Refinement			
N0. Diffraction peaks (Kα/Kβ)	110	110	110
N0. Background points	28	31	35
N0. Refined parameters	11	40	42
N0. atoms	0	0	0
Rp (%)	34.7	32.1	44.3
Rwp (%)	24.3	27.8	27.6
Rexp (%)	12.6	11.2	11.5
χ^2	3.74	6.19	5.77
Microstructure			
Crystallites size (nm)	14.3(1)	30.3(1)	26.9(1)

Table S2: Atomic ratio and stoichiometry of Mo carbides species calculated from XPS data.

	atomic %C sp^2 [a]	Mo/C [b]	Average stoichiometry (x) of Mo_xC species [c]	Mo^{2+}/Mo^{3+} [d]
Mo_2C-TMC	72.6	1.79	1.76	3.1
Mo_2C-HMC	79.5	1.66	1.58	1.4
Mo_2C-AHM	51.3	1.62	1.63	1.7

[a]*versus* total carbon at the surface. [b]ratio calculated by taking account the Mo carbides species only from C1s and Mo3d signal. [c]calculated from XPS atomic ratio from decomposition of Mo3d signal according to (%at.Mo^{2+}x2 + %at.Mo^{3+}) /(%at.Mo^{2+}+ %at.Mo^{3+}). [d]ratio calculated form atomic% of Mo^{2+} and Mo^{3+}

Table S3. Comparison of the electrocatalytic performance of Mo_2C-TMC with other HER catalysts reported in the literature in alkaline solutions.

Catalyst	Precursor	SSA ($m^2.g^{-1}$)	η_{10} (mV)	Tafel Slope ($mV.dec^{-1}$)	Electrolyte	Charge loading ($mg.cm^{-2}$)	Ref
Mo_2C-TMC	$(TBA)_2Mo_6Cl_{14}$ sucrose	103 ± 1	212	95	KOH 1 M	0.15	This work
Mo_2C@NCS	Ammonium molybdate, glucose, melamine, organic acid	101	147	77	KOH 1 M	0.25	1
β-Mo_2C nanotubes	$(NH_4)_6[Mo_7O_{24}].4H_2O$, hydrochloric dopamide	127	112	55	KOH 0.1 M	0.75	2
Mo_2C@NPC	PMo12, melamine, silicate spheres	47	121	73.5	KOH 1 M	0.57	3
α-Mo_2C	$MoCl_5$, urea	9	176	58	KOH 0.1 M	0.102	4
γ-Mo_2N	$MoCl_5$, urea	10	353	108	KOH 0.1 M		4
NiMo	$(NH_4)_6[Mo_7O_{24}].4H_2O$ and nickel nitrate	N/D	100	ND	KOH 2 M	0.1	5
Mo_2C	Glucose, NaCl and $(NH_4)_6Mo_7O_{24}{\cdot}4H_2O$	N/D	430	143	KOH 1 M	ND	6
Mo_2C-C	$(NH_4)_6Mo_7O_{24}{\cdot}6H_2O$, glucose and ethylene glycol	N/D	149	66	KOH 1 M	0.84	7
Mo/Mo_2C/N-CNFs	MoO_2(acac), cellulose actetate, polyacrylonitrile	N/D	162	47.9	KOH 1 M	1.68	8
Mo_2C-GNR	$(NH_4)_6[Mo_7O_{24}].4H_2O$, glucose, MWNTs	N/D	217	64	NaOH 1 M	0.28	9
Mo_2C@CS	$(NH_4)_6[Mo_7O_{24}].4H_2O$, glucose	816	178	50	KOH 1 M	0.4	10
Mo_2(CN)	$(NH_4)_6[Mo_7O_{24}].4H_2O$,	148	127	50	KOH 1 M	0.2	11

	melamine						

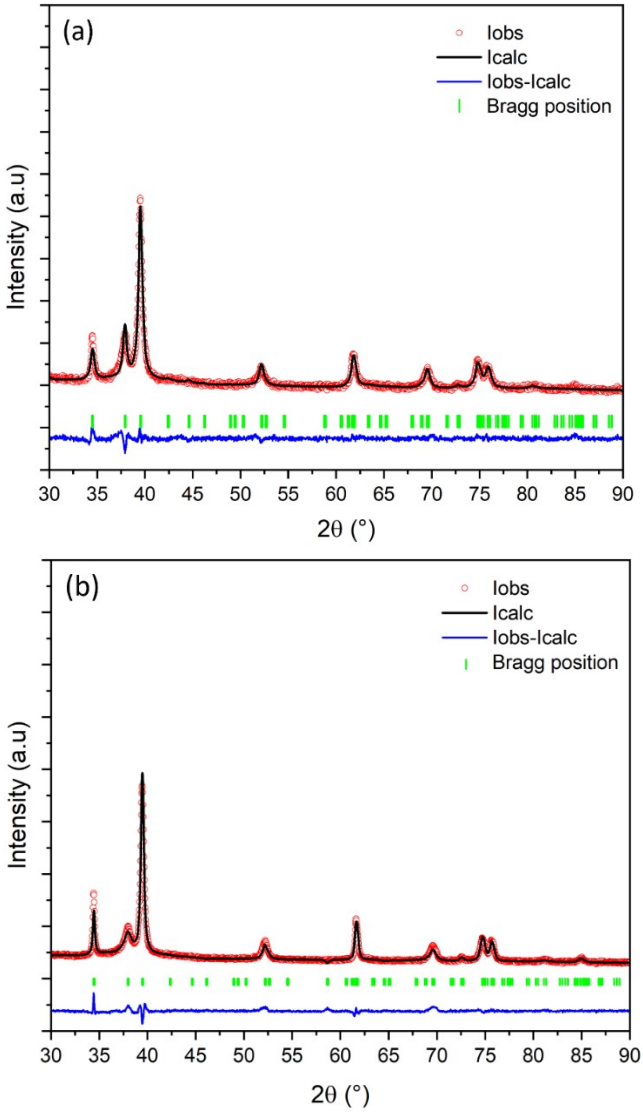
(a)
Iobs
Icalc
Iobs-Icalc
Bragg position
Intensity (a.u)
30 35 40 45 50 55 60 65 70 75 80 85 90
2θ (°)
(b)
Iobs
Icalc
Iobs-Icalc
Bragg position
Intensity (a.u)
30 35 40 45 50 55 60 65 70 75 80 85 90
2θ (°)

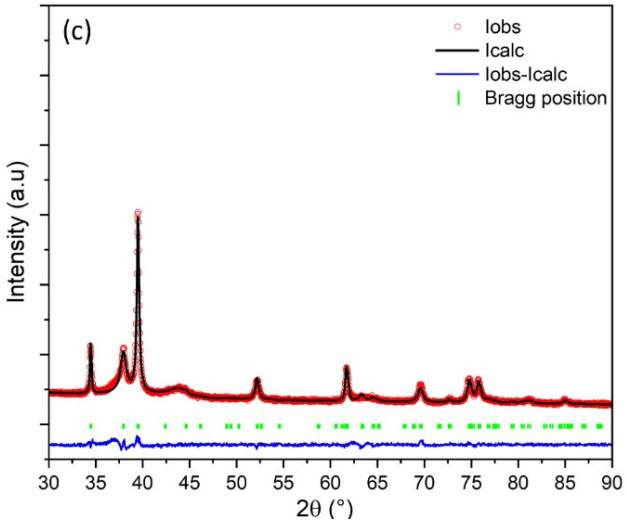

Fig. S1. LeBail refinement patterns for Mo_2C-AHM (a), Mo_2C-HMC (b) and Mo_2C-TMC (c): observed (red dotted line), calculated (black line) and difference X-ray powder diffraction profiles from the pattern matching plot obtained with the FullProf Suite Software. The vertical green markers correspond to the position of the Bragg reflections.

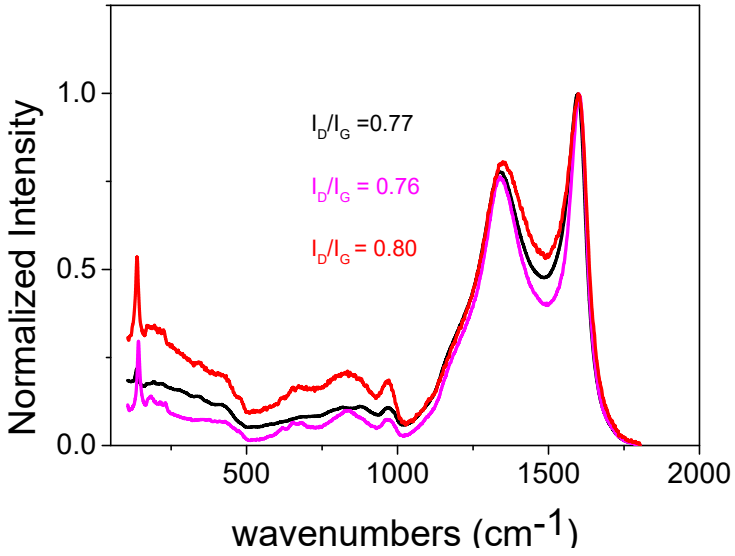

Fig. S2. Normalized Raman spectra for Mo_2C-TMC (black line); Mo_2C-HMC (magenta line) and Mo_2C-AHM (red line). The G and D bands due to carbon are clearly observed at 1597 and 1340-1348 cm^{-1}, respectively with a small downshift of the latter for the clusters- based compounds.

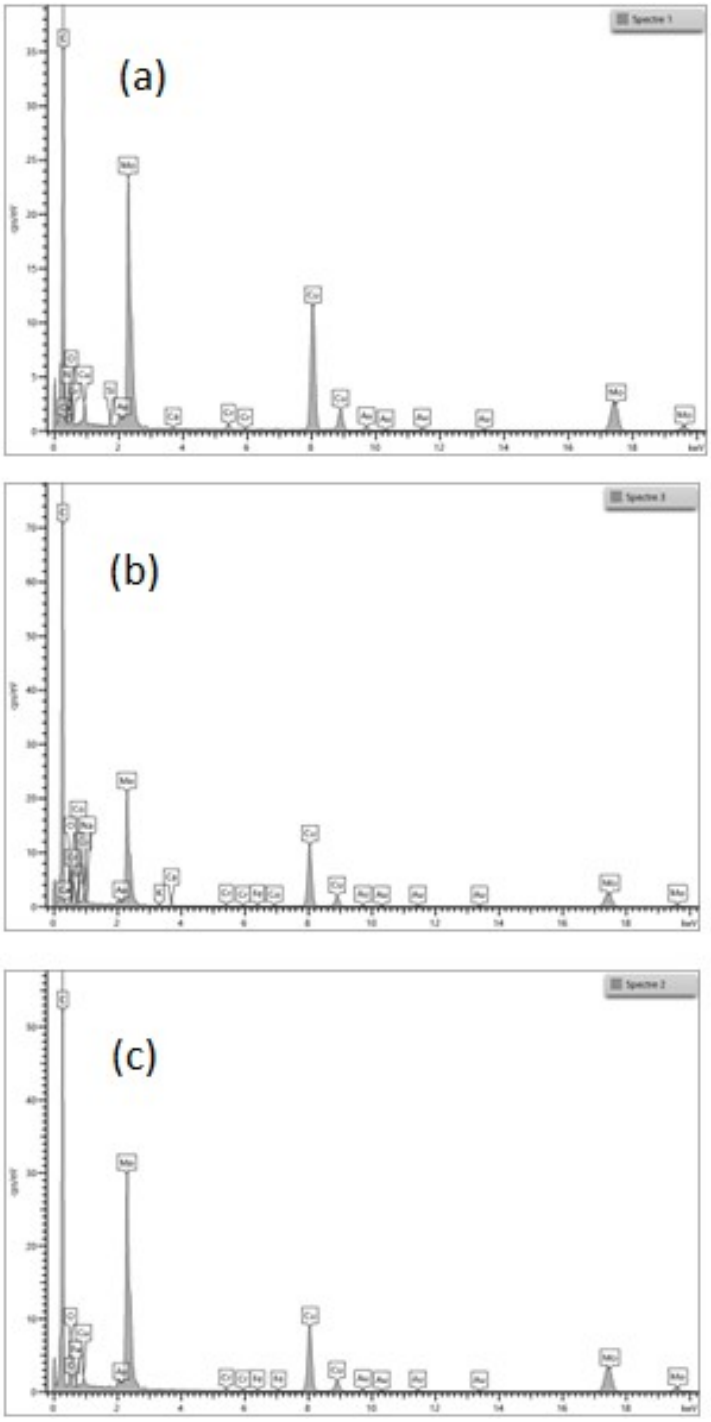

Fig. S3. EDS-TEM for the Mo_2C-AHM (a), Mo_2C-HMC (b) and Mo_2C-TMC (c). Cu, Fe, Cr and Au elements correspond to the material used for TEM analyses (Cu grid and specimen holder).

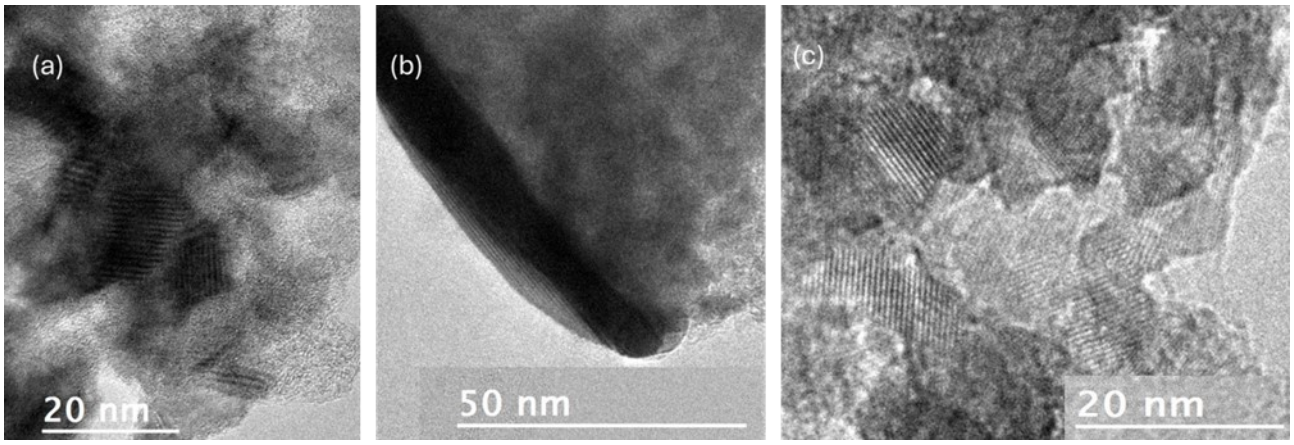

Fig. S4. HRTEM images of Mo_2C-AHM (a), Mo_2C-HMC (b) and Mo_2C-TMC (c) showing the lattice fringes of nanocrystals.

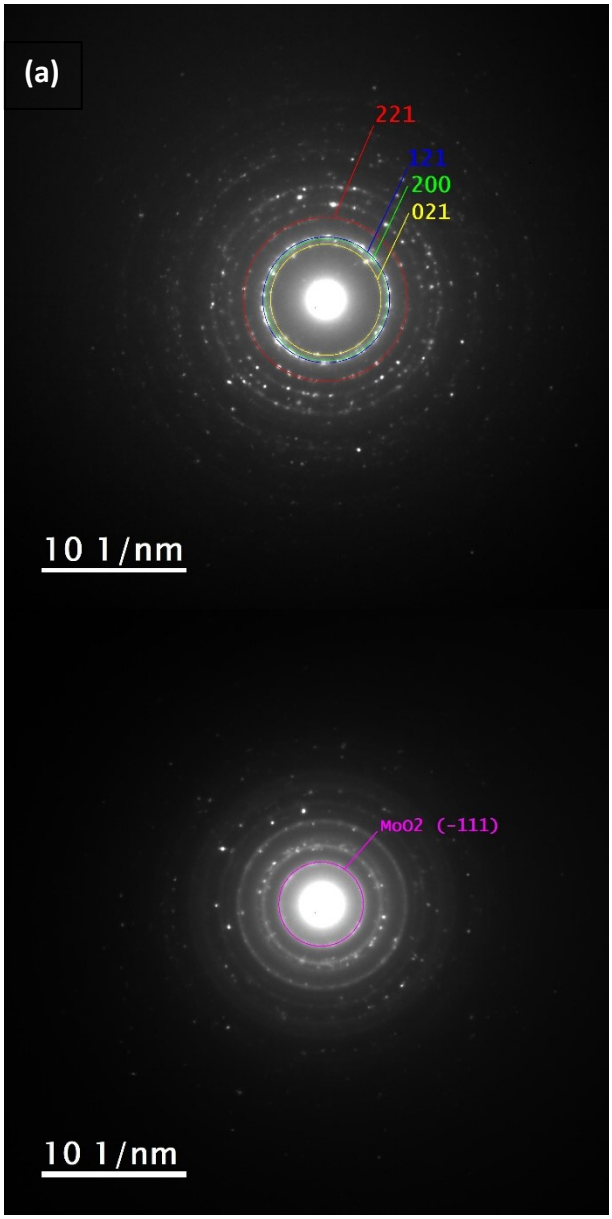

Fig. S5. Indexed SAED patterns displaying the (021), (200), (121) and (221) reflexions for Mo_2C-AHM (a), and (-111) reflexion of MoO_2 for Mo_2C-HMC (b).

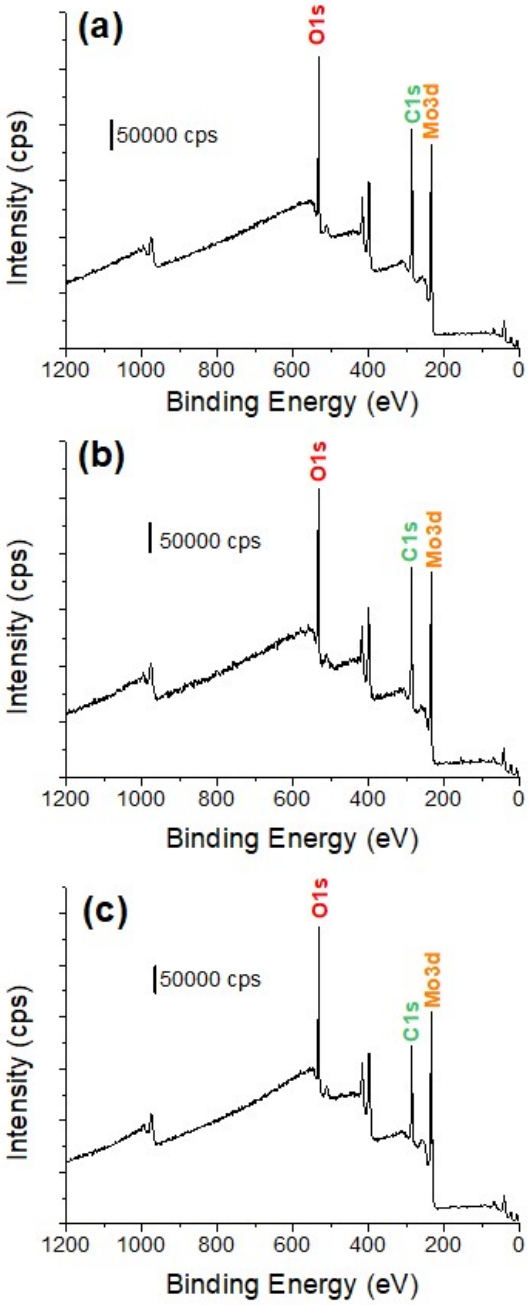

Fig. S6. XPS survey spectra for Mo_2C-TMC (a), Mo_2C-HMC (b) and Mo_2C-AHM (c)

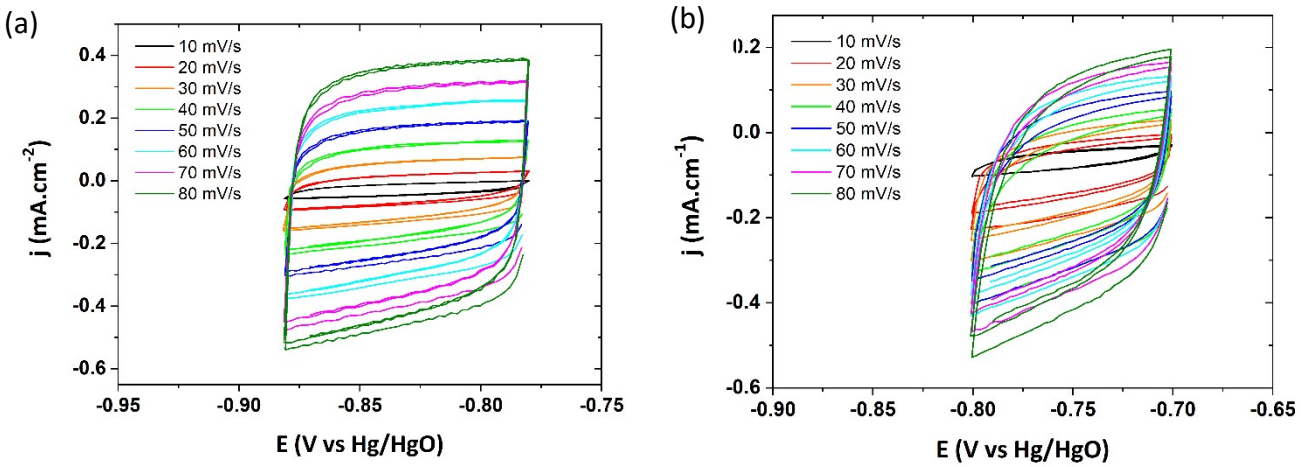

Fig. S7. Cyclic voltammetries in a non-faradaic region of the Mo_2C-AHM (a) before and (b) after 18 -chronopotentiometry at different scan rates (10, 20, 30, 40, 50, 60, 70 and 80 mV/s) in aqueous 1 M KOH.

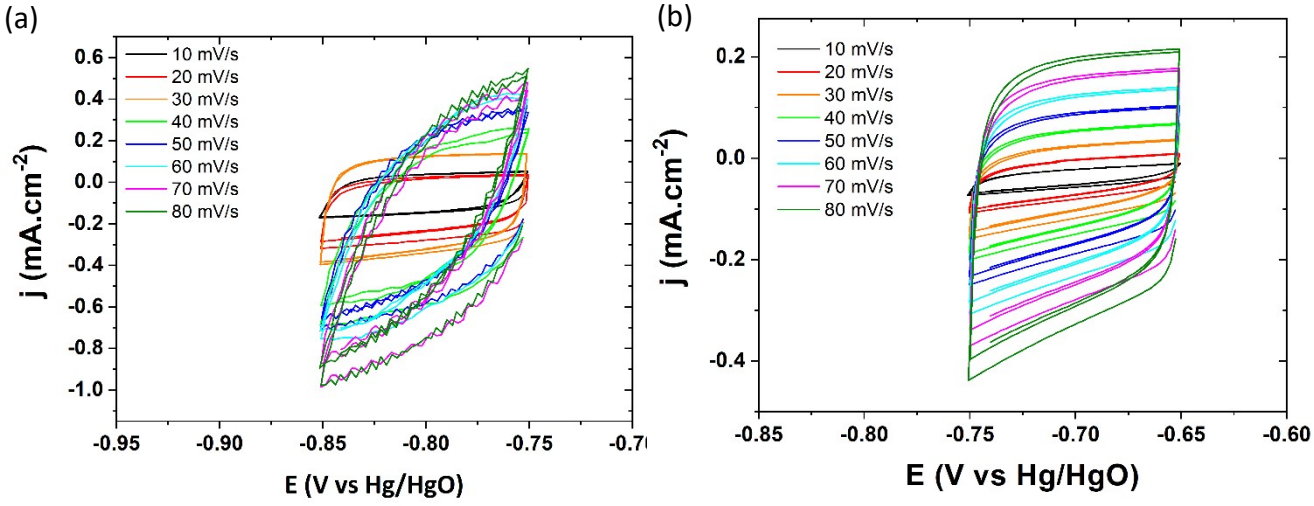

Fig. S8. Cyclic voltammetries in a non-faradaic region of the Mo_2C-HMC (a) before and (b) after 18h-chronopotentiometry at different scan rates (10, 20, 30, 40, 50, 60, 70 and 80 mV/s) in aqueous 1 M KOH.

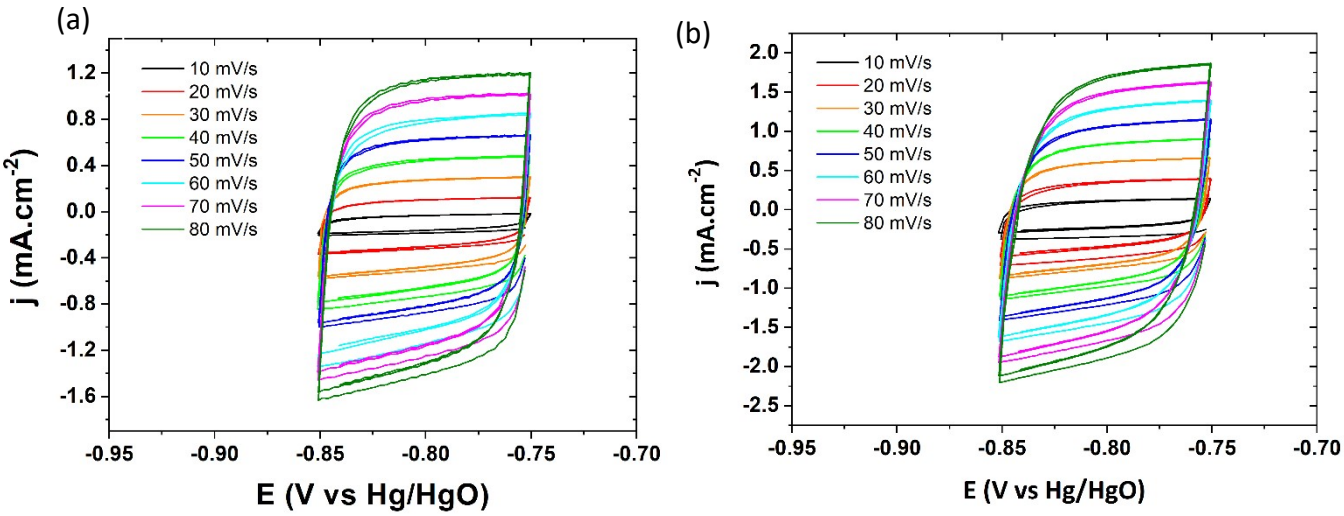

Fig. S9. Cyclic voltammetries in a non-faradaic region of the Mo_2C-TMC (a) before and (b) after 18h-chronopotentiometry at different scan rates (10, 20, 30, 40, 50, 60, 70 and 80 mV/s) in aqueous 1 M KOH.

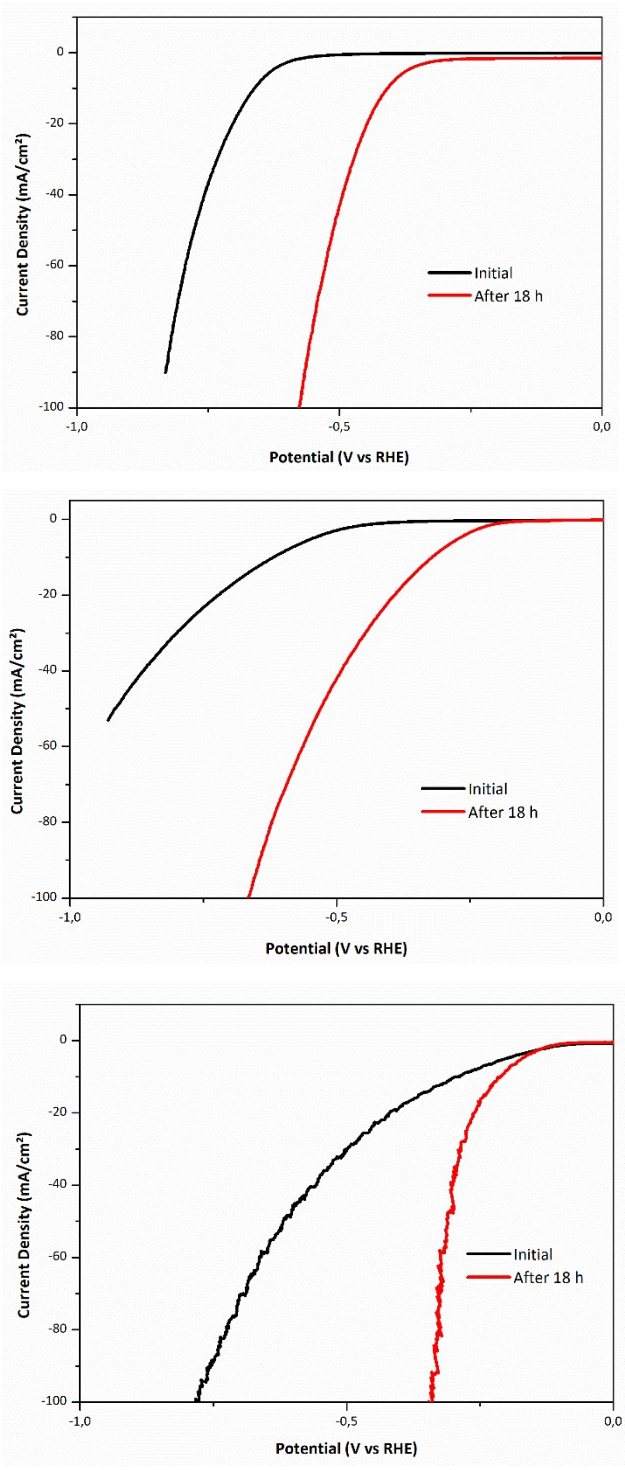

Fig. S10. iR-corrected HER polarization curves in aqueous 1 M KOH at 10 mV/s for Mo_2C-TMC (bottom), Mo_2C-HMC (middle), Mo_2C-AHM (top) before and after 18h-chronopotentiometry.

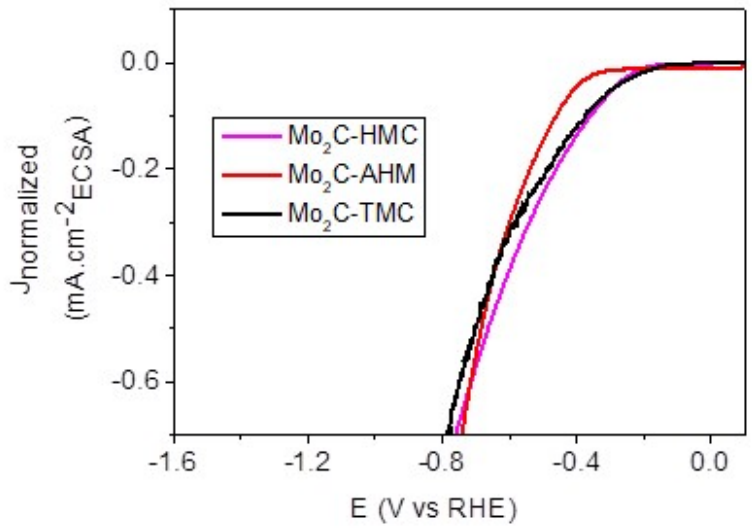

Fig. S11. iR-corrected HER polarization curves normalized by ECSA in aqueous 1 M KOH at 10 mV/s for Mo_2C-TMC, Mo_2C-HMC, Mo_2C-AHM after 18h-chronopotentiometry.

Note that ECSA value is roughly estimated here from C_{dl}/C_s where C_s is the specific capacitance. This value is taken equal to 0.040 mF/cm2 following Jaramillo et al.[12] this value is considered as a typical standard value (measured for metallic planar electrode) because we do not know the true Cs value. The electrochemical capacitance is estimated through CVs in non-Faradaic regions.

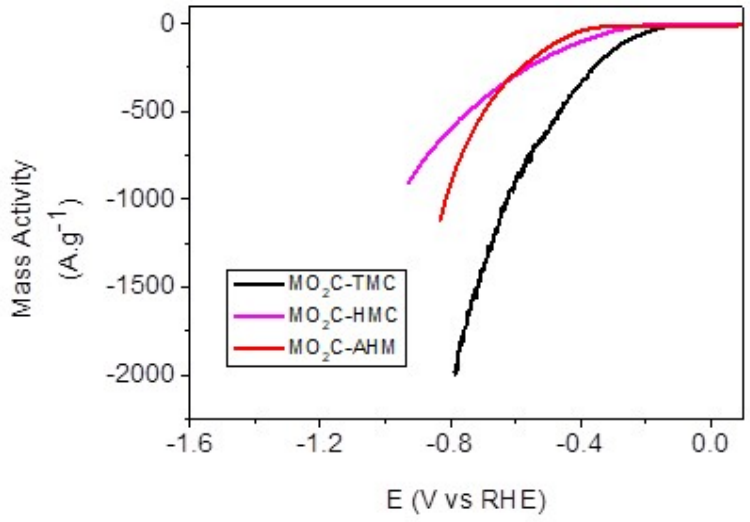

Fig. S12. iR-corrected HER polarization curves normalized by mass of the catalyst in aqueous 1 M KOH at 10 mV/s for Mo_2C-TMC, Mo_2C-HMC, Mo_2C-AHM after 18h-chronopotentiometry – Mass Activity.

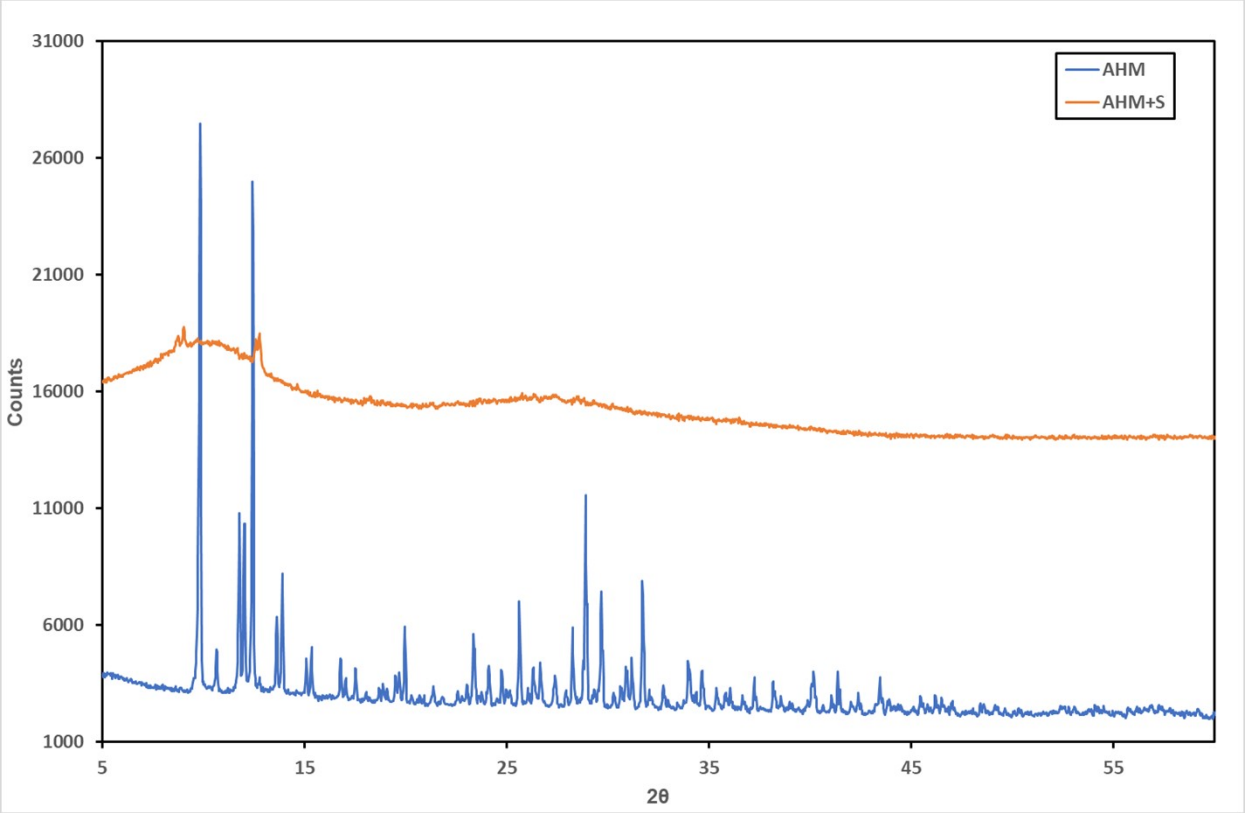

Fig. S13. Comparison between the XRD patterns of the AHM precursor (in blue) and that of the product (AHM + sucrose (S)) after treatment at 100°C (in orange).

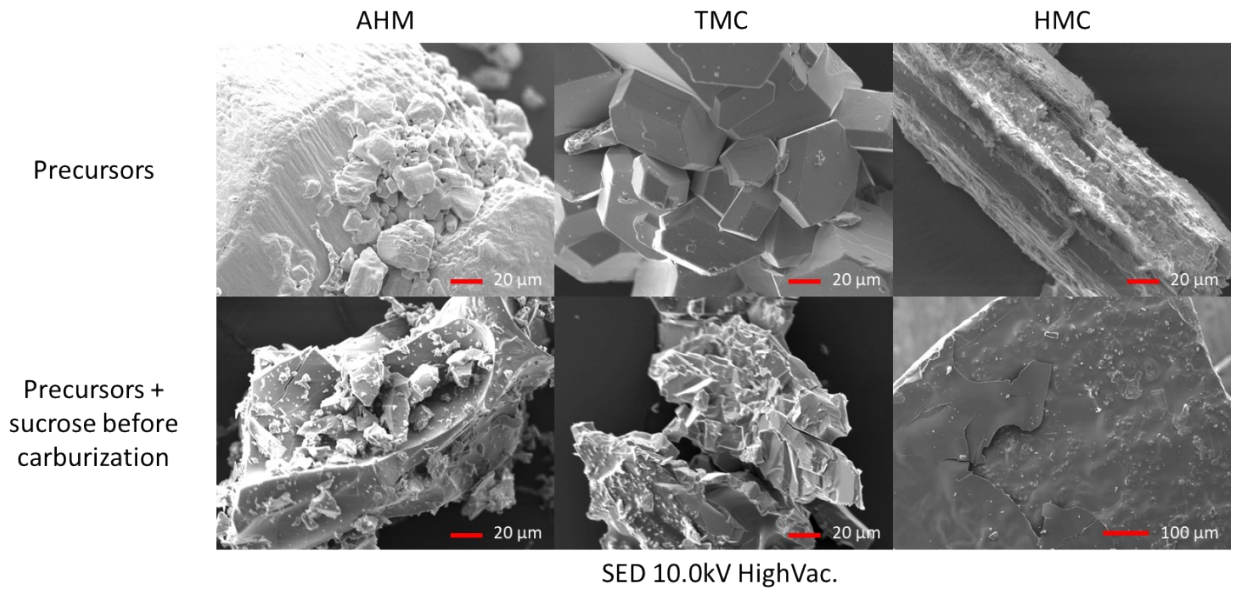

Fig. S14. SEM of the precursors (AHM, TMC and HMC) before (first line) and after (second line) sucrose addition

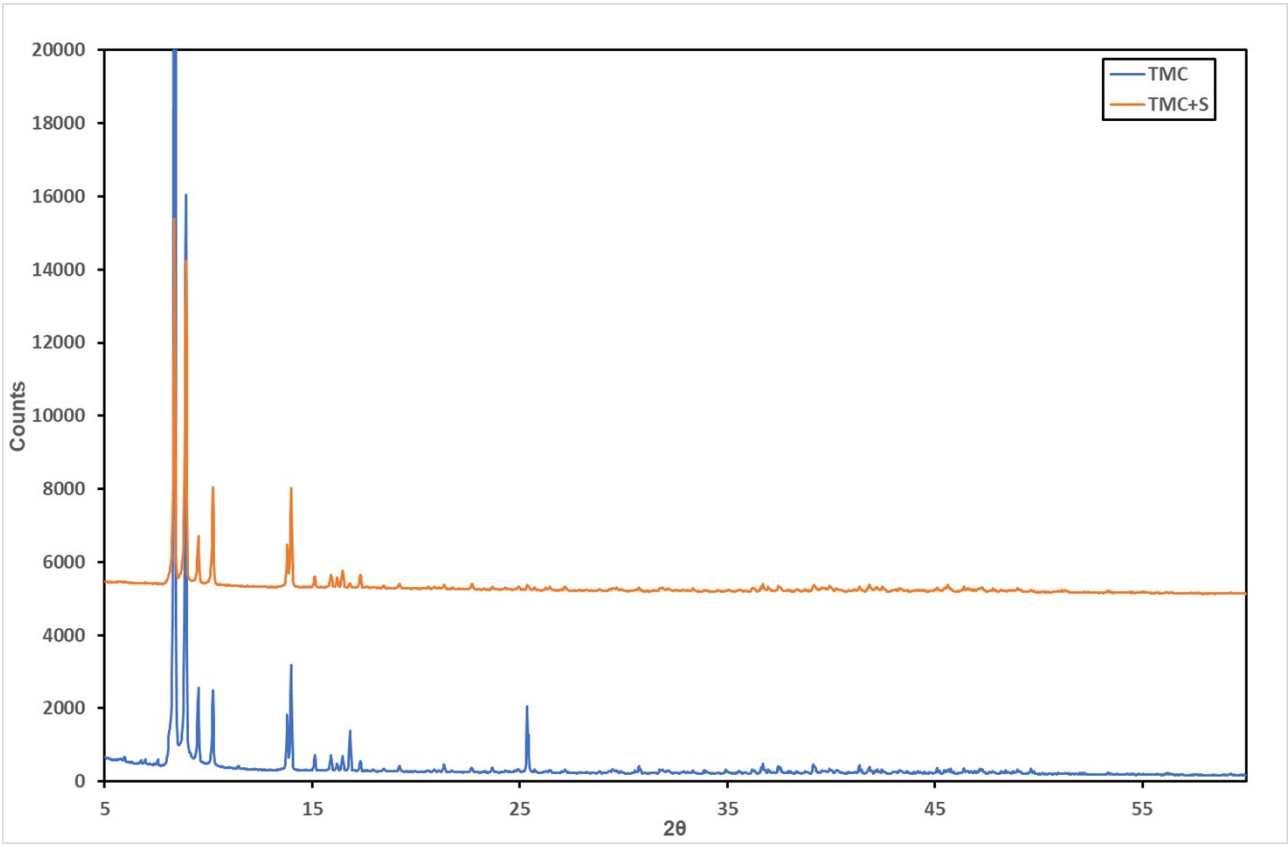

Fig. S15. Comparison between the XRD patterns of the TMC precursor (in blue) and that of the product (TMC + sucrose (S)) after treatment at 100°C (in orange).

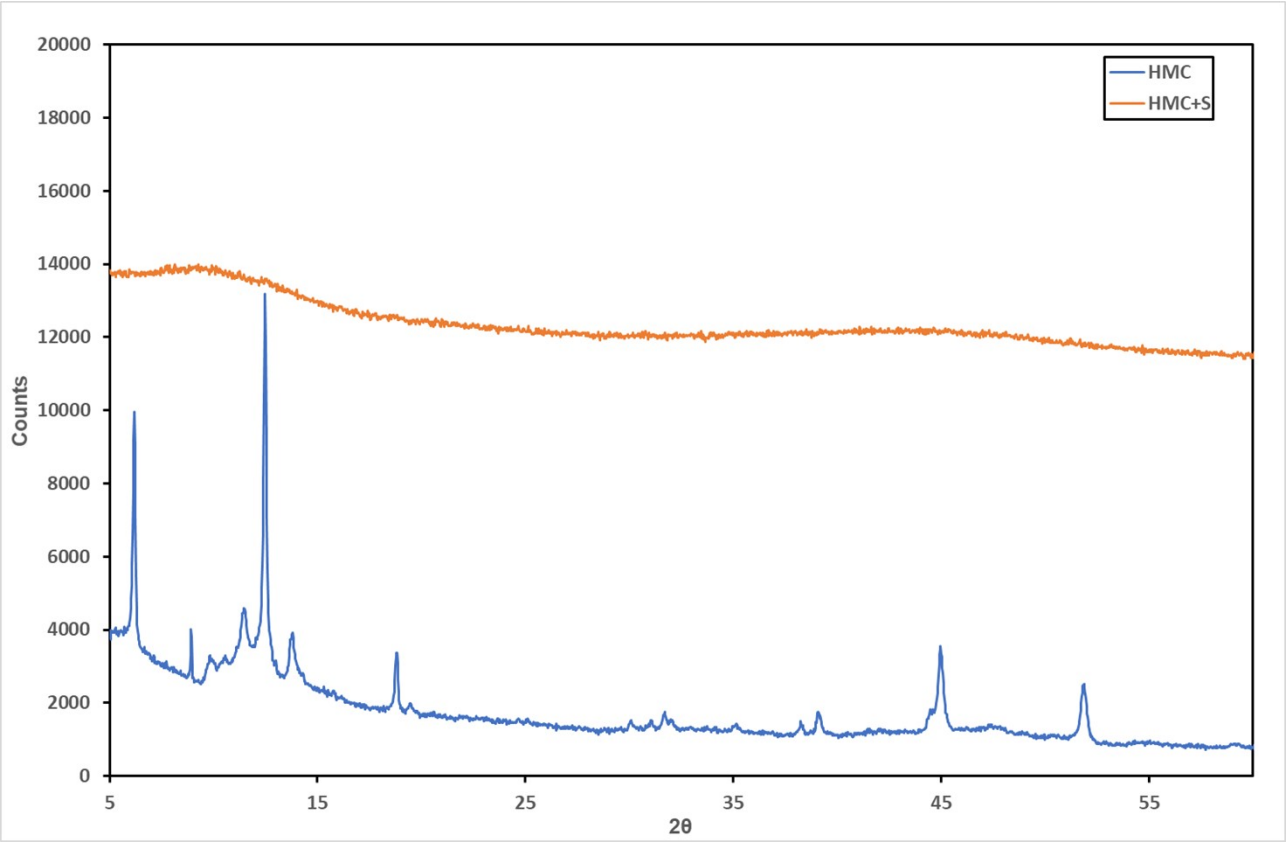

Fig. S16. Comparison between the XRD patterns of the HMC precursor (in blue) and that of the product (HMC + sucrose (S)) after treatment at 100°C (in orange).

References

[ ] J.T. Ren, L. Chen, D.D. Yang, Z.Y. Yuan, Molybdenum-Based Nanoparticles (Mo_2C, MoP and MoS_2) Coupled Heteroatoms-Doped Carbon Nanosheets for Efficient Hydrogen Evolution Reaction. Appl. Catal. B Environ., 2020, **263**, 118352.

[2] F.X. Ma, H.B. Wu, B.Y. Xia, C.Y. Bu, X.W. Lou, Hierarchical β-Mo_2C Nanotubes Organized by Ultrathin Nanosheets as a Highly Efficient Electrocatalyst for Hydrogen Production. Angew. Chem. Int. Ed., 2015, **54**, 15395-15399.

[3] K. Lan, L. Gong, M. Yang, X. Huang, P. Jiang, K. Wang, L. Ma, R. Li, Nitrogen and Phosphorus Dual-Doping Carbon Shells Encapsulating Ultrafine Mo_2C Particles as Electrocatalyst for Hydrogen Evolution. J. Colloid Interface Sci., 2019, **553**, 148 – 155.

[4] L. Ma, L.R. Ting, V. Molinari, C. Giordano, B.S. Yeo, Efficient Hydrogen Evolution Reaction Catalyzed by Molybdenum Carbide and Molybdenum Nitride Nanocatalysts Synthesized via the Urea Glass Route. J. Mater. Chem. A, 2015, **3**, 8361 – 8368.

[5] J.R. McKone, B.F. Sadtler, C.A. Werlang, N.S. Lewis, H.B. Gray, Ni–Mo Nanopowders for Efficient Electrochemical Hydrogen Evolution. ACS Catal., 2013, **3**, 166 – 169.

[6] C. Lv, J. Wang, Q. Huang, Q. Yang, Z. Huang, C. Zhang, Facile Synthesis of Hollow Carbon Microspheres Embedded with Molybdenum Carbide Nanoparticles as an Efficient Electrocatalyst for Hydrogen Generation. RSC Adv., 2016, **6**, 75870 – 75874.

[7] Z. Wu, J. Wang, R. Liu, K. Xia, C. Xuan, J. Guo, W. Lei, D. Wang, Facile Preparation of Carbon Sphere Supported Molybdenum Compounds (P, C and S) as Hydrogen Evolution Electrocatalysts in Acid and Alkaline Electrolytes. Nano Energy, 2017, **32**, 511 – 519.

[8] M. Li, H. Wang, Y. Zhu, D. Tian, C. Wang, X. Lu, Mo/Mo_2C Encapsulated in Nitrogen-doped Carbon Nanofibers as efficiently Integrated Heterojunction Electrocatalysts for Hydrogen Evolution Reaction in wide pH range, Appl. Surf. Sci., 2019, **496**, 143672.

[9] W. Gao, Y. Shi, Y. Zhang, L. Zuo, H. Lu, Y. Huang, W. Fan, T. Liu, Molybdenum Carbide Anchored on Graphene Nanoribbons as Highly Efficient All-pH Hydrogen Evolution Reaction Electrocatalyst, ACS Sustainable Chem. Eng., 2016, **4**, 6313 – 6321.

[10 H. Wang, Y. Cao, C. Sun, G. Zou, J. Huang, X. Kuai, J. Zhao, L. Gao, Strongly Coupled Molybdenum Carbide on Carbon Sheets as a Bifunctional Electrocatalyst for Overall Water Splitting, ChemSusChem, 2017, **10**, 3540 – 3546.

[11] C. Tang, Q. Hu, F. Li, C. He, X. Chai, C. Zhu, J. Liu, Q. Zhang, B. Zhu, L. Fan, Coupled Molybdenum Carbide and Nitride on Carbon Nanosheets: An Efficient and Durable Hydrogen

Evolution Electrocatalyst in both Acid and Alkaline media, Electrochim. Acta, 2018, **280**, 323 – 331.

[12] C.C.L. McCrory, S. Jung, J.C. Peters, T.F. Jaramillo, Benchmarking Heterogeneous Electrocatalysts for the Oxygen Evolution Reaction, J. Am. Chem. Soc. 2013, **135**, 45, 16977–16987